Wave runup video motion detection using the Radon Transform

Rafael Almar[1], Chris Blenkinsopp[2], Luis Pedro Almeida[3], Rodrigo Cienfuegos[4] and Patricio A. Catalan[5]

Abstract

A new method of runup detection from video imagery is introduced and validated at an energetic dissipative beach. The instantaneous waterline is detected from uprush and backwash by using the Radon Transform (RT). The method is compared to conventional color contrast method from RGB images and LiDAR measurements. In our observations, the RT shows better detection skill even for adverse conditions, such as those present on flat dissipative swash zones where contrast is reduced. Because the RT is a proxy of deeper waterline (~0.1 m) it is less sensitive to lack of contrast due to sand saturation. Moreover, since it is based on motion detection, it is less sensitive to changes in lighting conditions. Overall, the RT offers an attractive alternative for long term automated detection of the runup.

Keywords: Nearshore, Image processing, Radon Transform, LiDAR, Swash zone, Shoreline, Flow motion, Groundwater seepage

1. Introduction

Swash zone processes are a fundamental component of the beach system dynamics (Masselink and Hughes, 1998; Puleo et al., 2001). The swash zone links the terrestrial and marine environments and is an important source of sediment exchange between the surf zone and the

[1] IRD-LEGOS (CNRS/CNES/IRD/Université de Toulouse), Toulouse, France
[2] Univ. Bath, UK
[3] CNES-LEGOS, Toulouse, France
[4] DIHA-Pontificia Universidad Catolica de Chile, Santiago, Chile
[5] Dpt Obras Civiles,-Universidad Tecnica Federico Santa Maria, Valparaiso, Chile

subaerial beach (Masselink and Puleo, 2006). Given this relevance for nearshore hydrodynamics and morphodynamics, it is essential to have a monitoring system capable of capturing its large variability in space and time.

Remote sensing techniques, such as video imagery, are becoming more common in coastal studies and techniques have advanced greatly in recent years (Holman and Stanley, 2007; Holman and Haller, 2013). This type of remote sensing technique allows the automatic collection of a dense array of data, over a large range of temporal domains, ranging from wave-by-wave (seconds) to long term (years).

Video pixel array are usually sampled over time along cross-shore lines, allowing the creation of space-time maps of optical pixel intensity (usually termed timestacks) from which the swash can be identified (Aagaard and Holm, 1989; Guedes et al., 2013). Most existing methods of runup detection from video timestacks are based on pioneering studies of Holland & Holman (1993) and Holland et al. (1995, 2001) where the instantaneous waterline is defined as the interface between water and beach, and it is derived from optical information by the sharp Contrast in Colour band (CC). These methods are based on color contrast and not on hydrodynamical aspects. Thus, they can be sensitive to any changes in lighting conditions, sand and water color which may reduce the contrast, or induce false detection. Alas, they generally necessitate a time (to allow for changing lighting conditions throughout the daylight hours) and site specific calibration (Vousdoukas et al., 2014). For instance, the presence of wet sand creates a stark contrast with dry sand, and it is this boundary that can be erroneously identified as the shoreline. This is more frequent at dissipative beaches, and it often requires a manual correction of runup detection (Senechal et al., 2011; Guedes et al., 2013).

As an alternative to methods based on CC, the waterline can be defined from its motion, using the Radon Transform (Radon, 1917), by taking advantage of the spatio-temporal format from video timestacks, which is perfectly suited for this type of angle separation. The RT has recently been successfully applied to ocean waves, in particular for the detection of ship wave (Copeland et al., 1995) and more recently to nearshore wave dynamics (Yoo et al., 2011; Almar et al., 2014a), alongshore current (Almar et al., 2016) and swash motion (Zhang et al., 2009) but no attempt as conducted to estimate runup, despite the high potential of its use.

This paper introduces an alternative method for runup detection based on the RT and provides a quantitative validation through a comparison with LiDAR measurements conducted at a dissipative beach.

2. Runup detection principle using the Radon Transform

The RT $R(\rho,\theta)$ of a bidimensional field $\eta(x,y)$ (Radon, 1917; Deans, 1983; Duda and Hart, 1972) corresponds to a polar projection and can be defined as:

$$R(\rho,\theta) = \iint \eta(x,y)\delta(x\cos\theta + y\sin\theta - \rho)\mathrm{d}x\mathrm{d}y \quad (1)$$

where δ is the Dirac delta function, θ and ρ are the angle and distance from origin of the integration line defined as $\rho = x\cos\theta + y\sin\theta$. The origin is the center of the two-dimension field. The Radon transform $R(\rho, \theta)$ is defined for all possible values of θ from [0 to 180◦] and ρ from 0 to the diagonal length. The original field η(x,y) can be back projected using the Inverse Radon Transform at selected range of θ values :

$$\eta(x,y) = \iint R(\rho,\theta)\mathrm{d}\theta\mathrm{d}\rho \quad (2)$$

As an illustration, Figure 1 shows the application of the RT to a realistic cross-shore video timestack in the swash zone. The uprush and downrush motions are clearly visible in Figure 1a from the optical textured surface of turbulent swash flow. In the Radon space (Figure 1b), these motions with opposite direction show peaks at different values of θ, and alternate as the swash flow reverses; here negative and positive θ values respectively for uprush and donwrush. The incoming and outgoing motions are separated (see Figure 1a, red and blue features) by back projecting the original signal at negative and positive angles, respectively. In video timestack images, the runup is generally visible as a rapidly moving edge. Based on the RT, the runup can be then defined as the location of the maximum variance of the incoming (periods of uprush) and outgoing (periods of backwash) components. Our algorithm is implemented in Matlab, using on the Image Processing Toolbox, and is available from the authors upon request.

3. Field data

Data used in this paper were collected at Mataquito, Chile, on December 9th, 2012 (Figure 2.a, Cienfuegos et al., 2014). Mataquito is located in the Central coast of Chile. It is a black-colored, medium grain-size (D_{50} = 0.2 mm), intermediate to dissipative, micro-tidal beach, exposed to energetic waves. During the measurements, waves were moderate (H_s=1.5 m, T_p=14 s), the tide was low (-0.23 m) and the swash zone was located on the flat section of the lower intertidal profile (slope ~0.04, Figure 2.b).

A 2D scanning LiDAR (SICK LMS511-10100 Laser Measurement System) was deployed on a scaffolding tower, at an elevation 7.3 m above the beach in the upper swash to measure swash hydro- and morphodynamics (Blenkinsopp et al. 2010; Almeida et al. 2013; Vousdoukas et al., 2014; Brodie et al., 2015). Video swash monitoring was undertaken at 30 Hz using a SONY HDR-CX190 full HD 1920x1080 camcorder installed on a tripod. Timeseries of video pixel intensity were sampled along a cross-shore line, separated 3 m alongshore from LiDAR transect, and instrumented with metallic poles (Ibaceta et al., 2014). Rectification from image pixels into real world coordinates was accomplished through a direct linear transformation using DGPS ground control points (Holland et al., 2013) at the pole locations (Figure 2). The horizontal resolution obtained from the video data varied from less than 0.01 to 0.06 m along the cross-shore transect.

The ability of the RT method to detect runup is tested against concurrent LiDAR measurements over a 20-minute period obtained during the Mataquito experiment. The raw LIDAR measurements represent reflection of the laser beams from the beach topography as well as the water surface, without any distinction between the two. Water level is computed as water surface elevation above the bed, computed as the minimum level measured over the 20-min period. The runup edge is detected using a water level threshold, typically around 0.05-0.08 m (Blenkinsopp et al., 2016; Vousdoukas et al., 2014; Almeida et al., 2015), to cope with noise inherent to LiDAR measurements. Here, a 0.08 m threshold for LiDAR data for bed and water limit is used and is further discussed in Section 5. The conventional method based on colour contrast (CC) is also tested for comparison. There are several options for implementing CC methods and we chose here a simple but representative version based on the ratio of red-over-blue colour bands. A threshold standing for the maximum gradient is defined for the transition between water to

beach pixels, from blue and red dominated respectively, and this interface is tracked at each timeframe over the 20-min period.

4. Results

4.1 Validation of the Radon Transform method with LIDAR runup measurements

Taking the LiDAR as the baseline data, Figure 3 qualitatively shows that the RT approach captures the timing of individual swash events with far greater consistency than the conventional CC method, which struggles to distinguish between the shoreline during backwash and the groundwater seepage line as previously observed elsewhere (Vousdoukas et al., 2014). The CC approach appears incapable of resolving the rundown limit for the lighting conditions and mild beach slope investigated here and tends to detect the upper envelope of swash motions rather than the instantaneous shoreline. The RT can capture backwash, though typically gives rundown limits further landward than the LiDAR. While not in total agreement with the LiDAR data, this can also be due to the latter being less effective in detecting the shoreline during backwash (Blenkinsopp et al., 2016).

Table 1 shows that a better agreement is found between LiDAR and the RT than with CC, with correlation coefficients of 0.71 and 0.56 (both significant at 95% level), respectively and corresponding RMSE values of 0.1 and 0.4 m. The better performance of the RT approach is also evidenced by the swash parameters given in Table 1. It is noted that while both the CC and RT methods both underestimate the significant runup (R_{sig}), the RT value is closer in magnitude to the LiDAR value. As a consequence of the poor ability of the CC approach to resolve backwash discussed above, this approach estimates a mean swash period, T_m = 35 s, which is far larger than that obtained by either the LiDAR (T_m = 15.6 s) or RT (T_m = 13.4 s).

4.2 Depth identified by Radon Transform as the waterline

The RT detects the runup from its motion, which might not strictly coincide with the waterline limit. To estimate the water depth typically captured by the RT as the waterline, the depth threshold applied to the LiDAR data was varied in the range 0.02 to 0.2 m in Figure 4.a. Figure 4.b

shows correlation coefficients between RT and CC waterlines with different LIDAR depth thresholds. Levels lower than 0.05 have weak correlation primarily due to the difficulty of detecting such small water depths using LiDAR. When the water depth becomes very small, very few bubbles are present, which are required by the LiDAR to obtain valid signal returns. In addition, small wave-by-wave changes in bed elevation introduce uncertainty into depth estimations and lead to erroneous detections of the swash front. As previously found, a stronger correlation is obtained between LIDAR and RT (max. R^2=0.62) than with CC (max. R^2=0.4). Additionally, the RT offers better skills to pick the waterline defined at deeper water levels, with a maximum correlation around 0.1 m, than the CC, where the maximum is at 0.05 m.

5. Discussion

Weak correlation values are obtained between LiDAR and video waterlines at lower depths, in particular with CC. This could be somehow a bit misleading, not really because the LiDAR actually detects a short of thin slow moving backwash layer (which looks similar to the slow groundwater seepage line detected by the CC instead of backwash) but rather struggles to distinguish the runup front when the threshold is low, as observed for largest events in Figure 3 (which can also be caused by the 3-m separation between video and LiDAR transects). This because the LiDAR encounters difficulties with low depths as it becomes hard to distinguish between the bed/swash interface. This has the effect of slowing the backwash to groundwater desaturation with no assurance that the LiDAR is actually detecting anything real (Blenkinsopp et al., 2016).

The RT has a distinct behaviour than the CC and detects deeper waterline than the dry/wet limit: this because it is based on motion (i.e. flow) detection rather than colour contrast. Whereas no substantial differences are expected for swash statistics, the RT might be more suited when studying swash shape, such as asymmetry (Power et al., 2011) as it describes main flow behaviour instead of weak thin backwash limit. The potential of the RT can be extended in tracking instant surface current in the cross-shore direction. This is key in determining the flow velocities and reversal (Hugues and Baldock, 2004; Power et al., 2011) and associated sediment transport (Puleo et al., 2003). Noteworthy, similarly to what done for separating incoming and reflected waves in the surf zone by Almar et al. (2014), the RT can also be applied to swash zone in investigating swash-based reflection (Martin et al., 2017).

Puleo (2009) and Huisman et al. (2011) demonstrated that the optical trace of the groundwater seepage is clearly distinguishable on video images and this wet–dry boundary (such as often used in video shoreline-finding algorithms) is related to groundwater seepage on low-sloped beaches and may not be a good indicator of the position of the shoreline. The differences of behavior between the CC and RT to groundwater seepage and lighting conditions are illustrated in Figure 5 with their application to conventional tower-camera (Argus-like) video system timestacks at contrasted sites: a reflective (Grand Popo, Benin; slope=0.15), an intermediate (Nha Trang, Vietnam; slope=0.08) and a dissipative beach (Mataquito, Chile; slope=0.03). No substantial differences are seen between RT and CC methods at a steep reflective beach beach (correlation coefficient of 0.92), However, differences between the two methods raise when slope decreases at the intermediate (0.81) and dissipative beaches (0.59). The RT approach offers significant advantages at dissipative flat beaches where the CC can struggle to distinguish between the backwash and the more slowly moving groundwater seepage line (Figure 5.c). This shows the interest of combining the two methods to study dependencies between the swash and groundwater seepage, line as well as the waves, tides and rainfall (Huisman et al., 2011; Vousdoukas, 2014). This raises the question of the best waterline proxy to be used applying for the broadest range of conditions. Pixel intensity methods may be better suited for reflective beaches with turbulent white swash zone (Plant and Holman, 1997). This bright-band is generally absent on dissipative beaches (Plant et al., 2007) where CC methods with appropriate parametrization can retrieve both waterline and seepage line (Huisman et al., 2011; Vousdoukas, 2014) though it generally requires manual correction. More sophisticated methods based on swash-processes based definition generally offer better skills at complex intertidal or flat beaches (Aarninkhof et al., 2003; Almar et al., 2012). It is also noteworthy for automated detection that contrary to the CC, the RT is based on flow motion considerations so it is influenced to a lesser extent by varying lighting conditions, water and sand color, which offer significant advantages in long term monitoring.

6. Conclusions

A new video method based on the Radon Transform for detecting runup was introduced and tested at a dissipative beach, Mataquito, Chile. The ability of the RT to detect the instantaneous

shoreline was assessed by comparison to concurrent LiDAR measurements and compared to the commonly used color contrast method (CC), which defines the waterline from RGB colorbands contrast. In our observations, the RT shows better skill than the CC for the commonly adverse conditions of flat dissipative swash zones. Because the RT is based on motion detection it is better able than the CC approach to distinguish between backwash and the groundwater seepage line and is less sensitive to poor light conditions. Overall the RT offers an attractive alternative for long term automated detection of the runup.

Acknowledgments

Mataquito experiment was supported by Chilean Conicyt grants Fondecyt/1120878 and Fondap/15110017. This research has received support from French grants through ANR (COASTVAR: ANR-14-ASTR-0019). C.E. Blenkinsopp was supported by a University of Valparaiso visiting academic grant.

References

Aagaard, T. and Holm, J., 1989. Digitization of wave run-up using video records. J of Coastal Research, 5(3), 547-551.

Aarninkhof, S.G.J., Turner, I.L., Dronkers, T.D.T., Caljouw, M., Nipius, L., 2003. A video-based technique for mapping intertidal beach bathymetry. Coast. Eng. 49 (4), 275–289.

Almar, R., Michallet, H., Cienfuegos, R., Bonneton, P., Ruessink B.G. and Tissier, M., 2014. On the use of the Radon Transform in studying nearshore wave dynamics, Coastal Engineering, 92, 24-30

Almar R., Ranasinghe R., Senechal N., Bonneton P., Roelvink D., Bryan K., Marieu V., Parisot J.P. 2012. Video based detection of shorelines at complex meso- macrotidal beaches, Journal of Coastal Research. COAS_49646, vol. 28 (5), 1040-1048

Almeida LP, Masselink G, Russell PE, Davidson MA, 2015. Observations of gravel beach dynamics during high energy wave conditions using a laser scanner. Geomorphology, 228, 15-27

Blenkinsopp, C., Mole, M., Turner, I., & Peirson, W. 2010. Measurements of time-varying free-surface profile across the swash zone obtained using an industrial lidar. Coastal Engineering, 57, 1059–1065.

Blenkinsopp, C. E., Matias, A., Howe, D., Castelle, B., Marieu, V. and Turner, I. L., 2016. Wave runup and overwash on a prototype-scale sand barrier. Coastal Engineering, 113, pp. 88-103.

Brocchini, M., & Baldock, T. 2008. Recent advances in modeling swash zone dynamics: Influences of surf-swash interaction on nearshore hydrodynamics and morphodynamics. Reviews of Geophysics, 46(3), RG3003.

Brodie, K., B. Raubenheimer, Steve Elgar, R. Slocum, and J. McNinch, 2015. lidar and pressure measurements of inner -surf zone waves and setup, J. Atmospheric and Oceanic Technology

Cienfuegos, R., Villagran, M., Aguilera, J.-C., Cataln, P., Castelle, B., & Almar, R. 2014. Video monitoring and field measurements of a rapidly evolving coastal system: the river mouth and sand spit of the Mataquito river in Chile. Journal of Coastal Research, SI 70, 639–644.

Deans, S., 1983. The Radon transform and some of its applications, 1st Edition. John Wiley & Sons, New York, 289 p, ISBN 13: 9780471898047

Guedes, R., Bryan, K., & Coco, G. 2013. Observations of wave energy fluxes and swash motions on a low-sloping, dissipative beach. Journal of Geophysical Research, 118(7), 1–19.

Holland, K. T., and R. A. Holman 1993, The statistical distribution of swash maxima on natural beaches, J. Geophys. Res. ,87, 10,271–10,278

Holland, K. T. 1995. Foreshore dynamics: Swash motions and topographic interactions on natural beaches, Ph.D. thesis, Oreg. State Univ.,Corvallis, Oreg

Holland, K.T., J.A. Puleo and T.N. Kooney, 2001. Quantification of swash flows using video-based particle image velocimetry, Coastal Eng. 44, 65-77.

Holman, R. A., and A. H. Sallenger 1985, Setup and swash on a natural beach, J. Geophys. Res.,90, 945–953.

Holman RA, Stanley J. 2007. The history and technical capabilities of Argus. Coast. Eng. 54:477–91

Holman R, Haller MC (2013) Remote sensing of the nearshore. Ann Rev Mar Sci 5:95–113

Hughes, M. G., and T. E. Baldock (2004), Eulerian flow velocities in the swash zone: Field data and model predictions, J. Geophys. Res.,109,C08009, doi:10.1029/2003JC002213

Huisman, C.E., Bryan, K.R., Coco, G., and Ruessink, B.G., 2011. The use of video imagery to analyse groundwater and shoreline dynamics on a dissipative beach. Continental Shelf Research, 31 (16), 1728-1738

Ibaceta, R. Almar, R, Lefebvre, J.P., Senoo, T.M., Layrea, W.S., 2014. High frequency monitoring of swash hydromorphodynamics on a reflective beach (Grand Popo, Benin). International Conference on Coastal Engineering, Seoul, Corea, June 2014

Martins, K., Blenkinsopp, C.E, Almar, R., Zang, Z., 2017. On the influence of swash-based reflection on surf zone hydrodynamics: a wave-by-wave approach, Coastal Engineering, 122, 27-43

Masselink, G., & Hughes, M. 1998. Field investigation of sediment transport in the swash zone. Cont. Shelf Res., 18, 1179–1199.

Masselink, G. and Puleo, J.A., 2006. Swash zone morphodynamics. Continental Shelf Research, 26(5), 661-680

Plant, N. G., Holman, R. A., 1997. Intertidal beach profile estimation using video images. Mar. Geo. 140, 1-24.

Power, H., Holman, R., & Baldock, T., 2011. Swash zone boundary conditions derived from optical remote sensing of swash zone flow patterns. *J. of Geophysical Research*, *116*, 06007.

Puleo, J.A., Farquharson, G. Frasier, S.J., Holland, K.T., 2003. Comparison of optical and radar measurements of surf and swash zone velocity fields J. Geophys. Res. Oceans, 108, 3100, https://doi.org/10.1029/2002JC001483

Puleo, J.A., 2009. Tidal variability of swash-zone sediment suspension and transport. Journal of Coastal Research, 937–948 (2009)

Radon, J., 1917. "Über die Bestimmung von Funktionen durch ihre Integralwerte längs gewisser Mannigfaltigkeiten", Berichte über die Verhandlungen der Königlich-Sächsischen Akademie der Wissenschaften zu Leipzig, Mathematisch-Physische Klasse [Reports on the proceedings of the Royal Saxonian Academy of Sciences at Leipzig, mathematical and physical section], Leipzig: Teubner (69): 262–277; Translation: Radon, J.; Parks, P.C. (translator) (1986), "On the

determination of functions from their integral values along certain manifolds", IEEE Transactions on Medical Imaging, 5 (4): 170–176,

Senechal, N., Coco, G., Bryan, K., & Holman, R. 2011. Wave runup during extreme storm conditions. Journal of Geophysical Research - Oceans, 116, C07032.

Vousdoukas, M.I., 2014. Observations of wave run-up and groundwater seepage line motions on a reflective-to-intermediate, meso-tidal beach. Mar. Geol., 350, 52–70 https://doi.org/10.1016/j.margeo.2014.02.005

Vousdoukas, M., Kirupakaramoorthy, T., Oumeraci, H., de la Torre, M., Wubbold, F., Wagner, B., & Schimmels, S., 2014. The role of combined laser scanning and video techniques in monitoring wave-by-wave swash zone processes. Coastal Engineering, 83, 150–165

Yoo, J., Fritz, H., Haas, K., Work, P., and Barnes, C., 2011. Depth inversion in the surf zone with inclusion of waves non-linearity using video-derived celerity. J. Waterw. Port Coastal Oc. Eng., 137(2), 95-106

Zhang, S., Zhang, C., Qi, Z., 2009. Waves swash velocity estimation using ridgelet transform. In: 9th Int. Conf. Electronic Meas. & Instr. ICEMI 09. 1078-1081

Figure captions

Figure 1. a) Aerial view of Mataquito beach, Chile with studied cross-shore transect (dashed line) and b) surveyed bathymetric profile, solid and dashed blue lines stand for mean sea level, max and min spring tidal elevations, respectively. The local slopes on the upper and lower intertidal parts of the beach profile were 0.06 and 0.03 respectively. In c) and d) the deployment of the LiDAR and concurrent video camera and swash poles are shown.

Figure 2. Illustration of the runup detection using the Radon Transform. a) Example of video timestack image from Mataquito. The superimposed red and blue patches indicate incoming and outgoing pixel intensity components, respectively. The black line indicates the location of the estimated instantaneous waterline position. b) Corresponding angular density (signal

integration along angled lines -Eq1-, see Almar et al. (2014) for details on the RT) computed from the Radon Transform. Positive angles are offshore oriented and negative angles are onshore oriented.

Figure 3. Timeseries of horizontal runup from Colour Contrast (CC), Radon Transform (RT) and LIDAR (0.08 m threshold) superimposed on the cross-shore pixel timestack. Of note, the uprush limit goes beyond the limit of the images for quite a few of the swashes.

Figure 4. a) Illustration of the cross-shore evolution of depth from LiDAR where the colorscale and white contours represent water free surface elevation; and b) coefficient of determination R^2 of LiDAR waterline with RT and CC, for different LIDAR reference water levels.

Figure 5. Illustration of runup detection with RT (red) and CC (blue) methods. Video cross-shore timestacks from a reflective beach (Grand Popo, Benin; up panel), intermediate beach (Nha Trang, Vietnam; mid panel) and a dissipative beach (Mataquito, Chile; low panel).

Figure1

Click here to download high resolution image

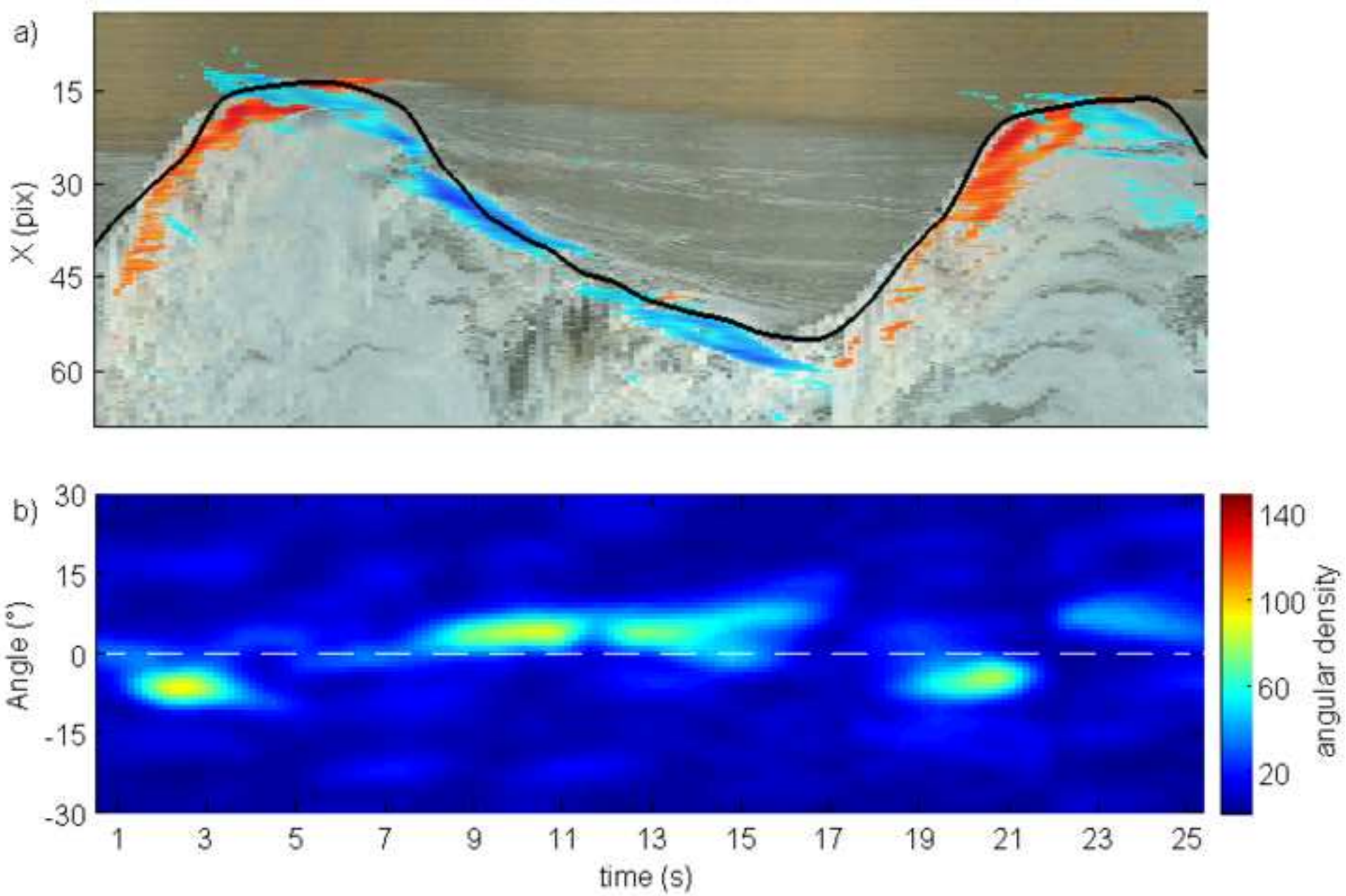

Figure2

Click here to download high resolution image

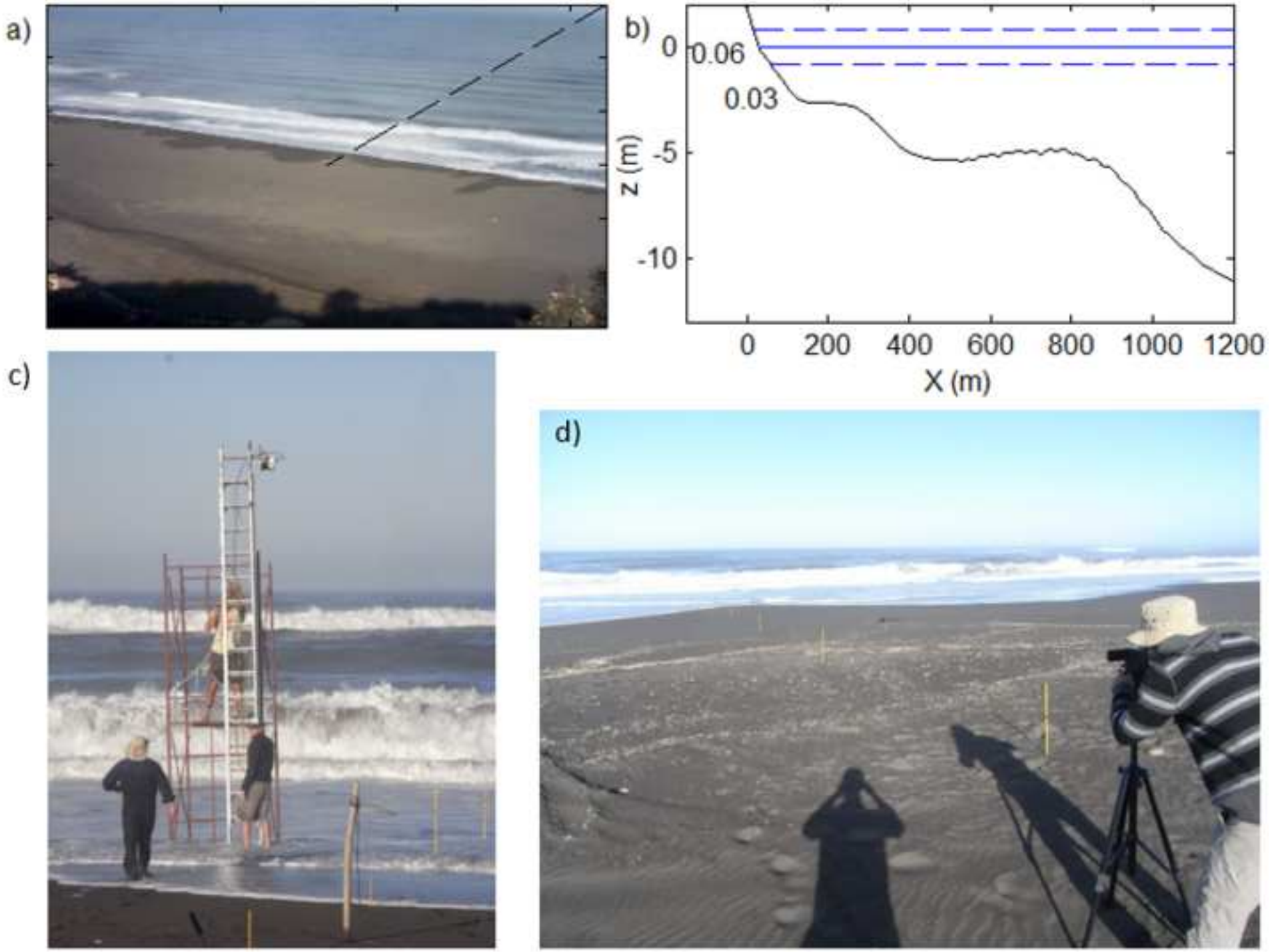

Figure3
Click here to download high resolution image

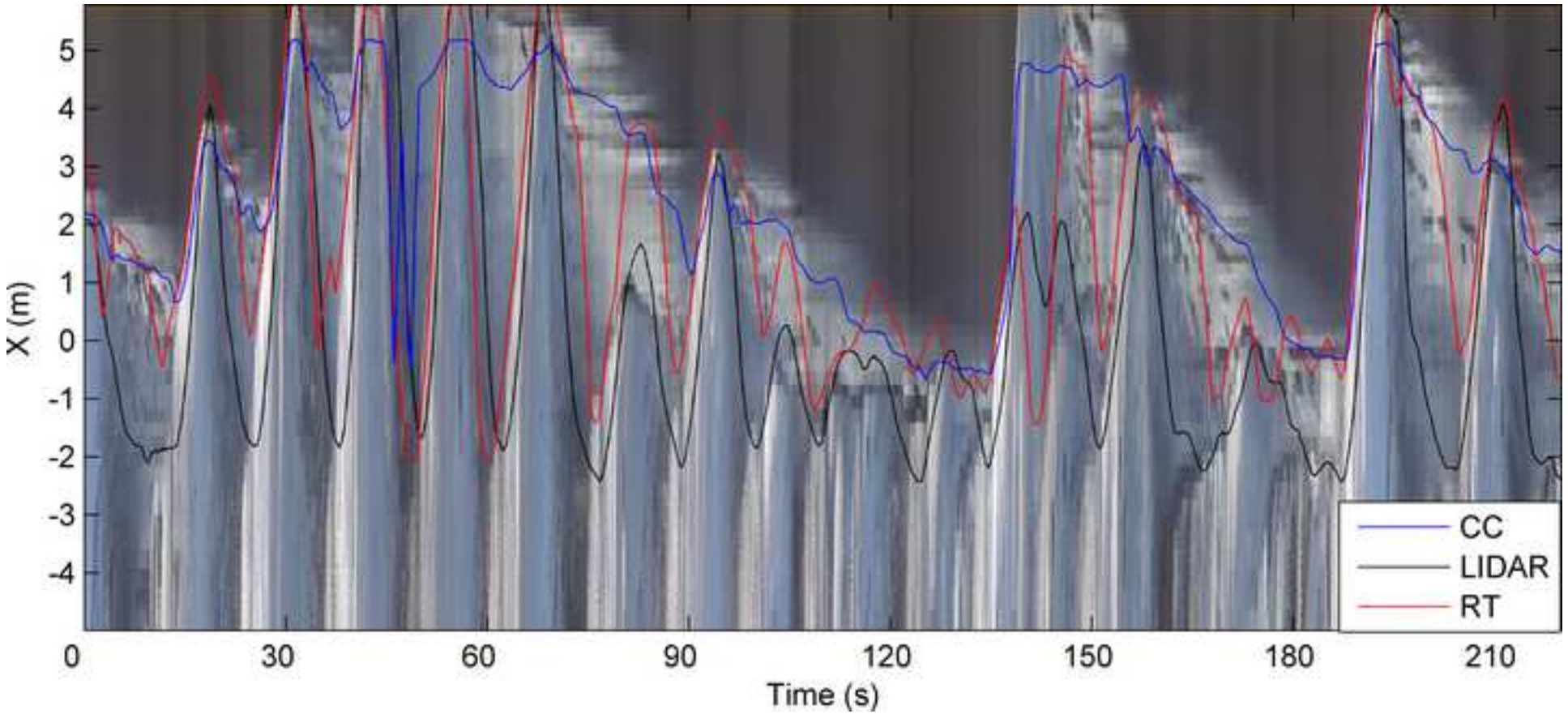

Figure4

Click here to download high resolution image

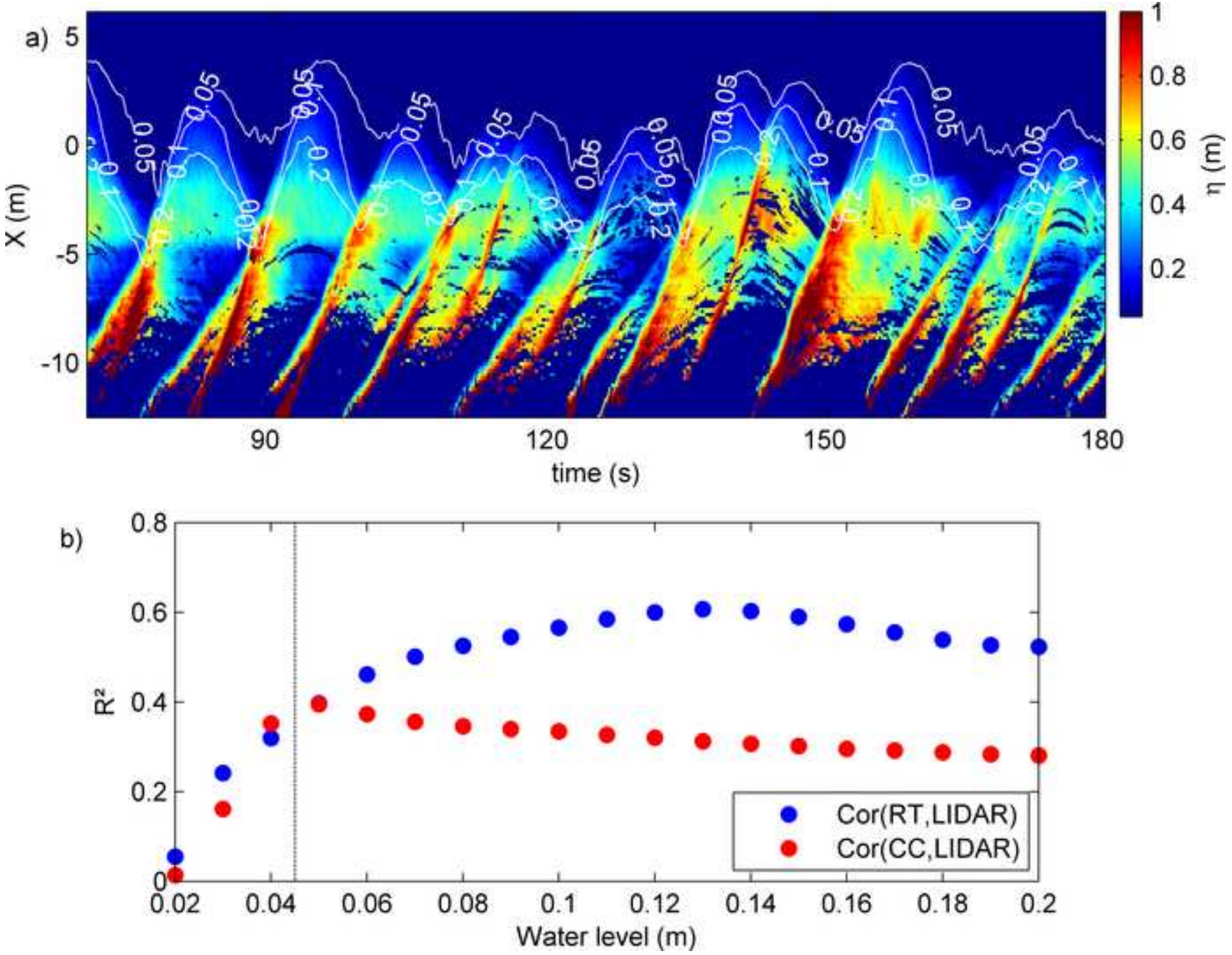

Figure5

Click here to download high resolution image